High-Pressure Sequence of $Ba_3NiSb_2O_9$ Structural Phases: New $S = 1$ Quantum Spin Liquids Based on Ni^{2+}

J. G. Cheng,[1] G. Li,[2] L. Balicas,[2] J. S. Zhou,[1] J. B. Goodenough,[1] Cenke Xu,[3] and H. D. Zhou[2,*]

[1]*Texas Materials Institute, University of Texas at Austin, Texas 78712, USA*
[2]*National High Magnetic Field Laboratory, Florida State University, Tallahassee, Florida 32306-4005, USA*
[3]*Department of Physics, University of California, Santa Barbara, California 93106, USA*
(Received 7 June 2011; published 4 November 2011)

Two new gapless quantum spin-liquid candidates with $S = 1$ (Ni^{2+}) moments: the 6*H*-B phase of $Ba_3NiSb_2O_9$ with a Ni^{2+}-triangular lattice and the 3C phase with a $Ni_{2/3}Sb_{1/3}$-three-dimensional edge-shared tetrahedral lattice were obtained under high pressure. Both compounds show no magnetic order down to 0.35 K despite Curie-Weiss temperatures θ_{CW} of -75.5 (6*H*-B) and -182.5 K (3C), respectively. Below ~ 25 K, the magnetic susceptibility of the 6*H*-B phase saturates to a constant value $\chi_0 = 0.013$ emu/mol, which is followed below 7 K by a linear-temperature-dependent magnetic specific heat (C_M) displaying a giant coefficient $\gamma = 168$ mJ/mol K². Both observations suggest the development of a Fermi-liquid-like ground state. For the 3C phase, the $C_M \propto T^2$ behavior indicates a unique $S = 1$, 3D quantum spin-liquid ground state.

A quantum spin liquid (QSL) is a ground state where strong quantum-mechanical fluctuations prevent a phase transition towards conventional magnetic order and make the spin ensemble to remain in a liquidlike state [1,2]. So far, various gapped spin liquids have been found in dimerized spin systems and spin ladders [3–11]. However, topological and gapless spin liquids are much less well-understood in dimensions higher than one. Most of the gapless QSL candidates studied to date are two-dimensional frustrated magnets composed of either a triangular lattice of $S = 1/2$ dimers, such as the organic compounds κ-(BEDT-TTF)$_2$Cu$_2$(CN)$_3$ [12,13] or EtMe$_3$Sb[Pd(dmit)$_2$]$_2$ [14,15], or of a kagome lattice of Cu^{2+} ($S = 1/2$) ions, such as the $ZnCu_3(OH)_6Cl_2$ [16,17], $BaCu_3V_2O_8(OH)_2$ [18], and $Cu_3V_2O_7(OH)_2 \cdot 2H_2O$ [19] compounds.

However, whether a gapless QSL can be realized in systems with larger spins, e.g., $S = 1$, especially in systems with a three-dimensional (3D) lattice, is still a matter of debate. For example, the $S = 1$ material $NiGa_2S_4$ [20] with a triangular lattice develops quadrupolar order [21,22], while so far all the 3D gapless QSL candidates studied to date, such as $Na_4Ir_3O_8$ with Ir^{4+} ions [23], are either $S = 1/2$ or effective $S = 1/2$ systems due to strong spin-orbit coupling. Therefore, the present challenge is to find additional model compounds to test current theories for gapless QSLs. The key to find a new QSL candidate is to construct a geometrically frustrated lattice with specific magnetic ions. A commonly used method to design and discover new materials is to pursue chemical substitutions, although the application of high pressures is also an alternative way to transform crystalline structures and discover new phases which has not been widely used for synthesizing new frustrated magnets. Here, we followed

the second route to synthesize frustrated magnets $Ba_3NiSb_2O_9$ displaying the unique physical properties shown below.

The ambient pressure 6*H*-A phase of $Ba_3NiSb_2O_9$ was synthesized through a conventional solid-state reaction. Its x-ray diffraction (XRD) pattern [recorded at room temperature with Cu K$_\alpha$ radiation, Fig. 1(a)] shows a single phase having the hexagonal space group $P6_3/mmc$. The obtained lattice parameters $a = 5.8376(5)$ Å and $c = 14.4013(1)$ Å agree well with previously reported values [24,25]. The structure of the 6*H*-A phase [Fig. 1(d)] consists of dimers of face-sharing Sb_2O_9 octahedra linked by their vertices to single corner-sharing $NiO_{6/2}$ octahedra along the c axis. The Ni^{2+} ions occupy the 2*a* Wyckoff site to form a two-dimensional (2D) triangular lattice in the ab plane [Fig. 1(g)], which is separated by two nonmagnetic Sb layers.

The 6*H*-B phase of $Ba_3NiSb_2O_9$ was obtained by treating the 6*H*-A phase at 600 °C under a pressure of 3 GPa for 1 h in a Walker-type multianvil module (Rockland Research Co.). Its XRD pattern [Fig. 1(b)] is different from that of 6*H*-A phase and can be satisfactorily indexed as a distinct hexagonal space group, i.e., the $P6_3mc$ with $a = 5.7923(2)$ Å and $c = 14.2922(7)$ Å, respectively. In this structure [Fig. 1(e)], the dimers of the face-sharing $NiSbO_9$ octahedra (instead of the Sb_2O_9 octahedra as for the 6*H*-A phase) are linked by their vertices to single corner-sharing $SbO_{6/2}$ octahedra along the c axis. In the well-ordered $NiSbO_9$ octahedra, the Ni^{2+} ions occupy the 2*b* Wyckoff sites, which still form a triangular lattice in the ab plane. For the 6*H*-A phase, the layers of the Ni triangular lattice are exactly on top of each other along the c axis. However, for the 6*H*-B phase, the nearest two layers of the Ni triangular lattice are displaced with respect to
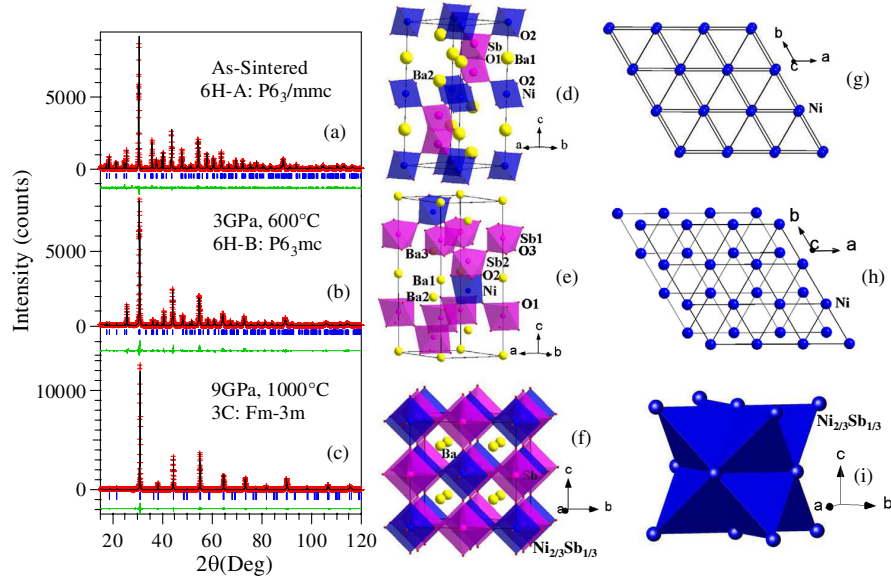
FIG. 1 (color online).   Powder XRD patterns (crosses) at 295 K for the $Ba_3NiSb_2O_9$ polytypes: (a) 6H-A, (b) 6H-B, and (c) 3C. Solid curves are the best fits obtained from Rietveld refinements using FULLPROF. Schematic crystal structures for the $Ba_3NiSb_2O_9$ polytypes: (d) 6H-A, (e) 6H-B, and (f) 3C; red octahedra represent Sb(M′) sites, and blue octahedra represent $Ni_{2/3}Sb_{1/3}$(M) sites. Magnetic lattices composed of Ni^{2+} ions for the $Ba_3NiSb_2O_9$ polytypes: (g) 6H-A, (h) 6H-B, and (i) 3C.

each other in a way that the Ni ion in one layer is projected towards the center of the triangle formed by the Ni ions in the adjacent layers along the c axis, as shown in Fig. 1(h). The instability of the 6H-A phase should arise from the fact that high pressures tend to reduce the Sb^{5+}-Sb^{5+} distance and therefore partially relieve strong electrostatic repulsion by exchanging Ni with one of the Sb atoms. Battle *et al.* reported a similar structure for the 6H-B phase [26], but with no physical characterization.

With increasing pressure we observed an additional phase transformation to a cubic perovskite structure. This 3C phase was obtained under 9 GPa and at a temperature of 1000 °C kept for 30 min. Its XRD pattern [Fig. 1(c)] is best described as a double perovskite in a $Ba_2MM'O_6$ model with the cubic space group $Fm3m$ having a lattice parameter $a = 8.1552(2)$ Å. The refinement shows a full-ordered arrangement of $Ni_{2/3}Sb_{1/3}$ and Sb atoms at the M and M′ sites [Fig. 1(f)], respectively. Therefore the $Ni_{2/3}Sb_{1/3}$ sites form a network of edge-shared tetrahedra, as shown in Fig. 1(i). Instead of adopting a primitive perovskite structure in which the Ni^{2+} and Sb^{5+} ions are randomly distributed, the preferred double-perovskite structure should be attributed to the large difference in charges between the Ni^{2+} and the Sb^{5+} ions.

All three samples are insulators with the room temperature resistance higher than 20 MΩ. The dc magnetic susceptibility [$\chi(T)$, Fig. 2] for all three compounds was measured under a field $H = 5000$ Oe. For each compound, one does not observe any difference between the data measured under zero-field-cooled and that measured under field-cooled conditions. The 6H-A sample exhibits

a cusplike anomaly at the antiferromagnetic ordering temperature $T_N = 13.5$ K, as previously reported [25]. On the other hand, neither the 6H-B nor the 3C phase show any sign of long-range magnetic order down to 2 K. For the 6H-B phase, we have subtracted the Curie contribution provided by 1.7% Ni^{2+} of orphan spins from the as-measured data. This percentage of Ni^{2+} orphan spins was calculated from fitting the specific-heat data [27]. After this subtraction, $\chi(T)$ for the 6H-B phase (open squares in Fig. 2) basically saturates below 25 K with a saturation
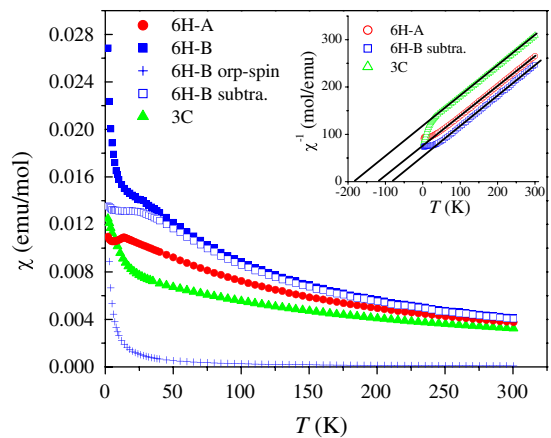
FIG. 2 (color online).   (a) Temperature dependencies of the dc magnetic susceptibility (χ) for the $Ba_3NiSb_2O_9$ polytypes. Inset: Temperature dependencies of $1/\chi$. The solid lines on $1/\chi$ data represent Curie-Weiss fits. For 6H-B phase, χ (open squares) is obtained by subtracting 1.7% Ni^{2+} orphan spin's contribution (crosses) from the as-measured data (solid squares).

value $\chi_0 \sim 0.013$ emu/mol. The fittings of the high-temperature region of $\chi^{-1}(T)$ to the Curie-Weiss law show that all three compounds have the same value for the effective moment, $\mu_{\mathrm{eff}} \sim 3.54 \mu_B$, as seen from the fact that all three $\chi^{-1}(T)$ curves are basically parallel to each other (inset in Fig. 2). This value gives a g factor of 2.5, which is close to the typical value for Ni^{2+} ions with spin-orbital coupling [28]. The Curie-Weiss temperatures θ_{CW} obtained for the 6H-A, 6H-B, and 3C phases are $-116.9(4)$, $-75.6(6)$, and $-182.5(3)$ K, respectively, indicating dominant antiferromagnetic interactions for all compounds.

The magnetic specific heat (C_M, Fig. 3) for each compound was obtained by subtracting the heat capacity of the nonmagnetic compound $Ba_3ZnSb_2O_9$ ordered in the 6H-A, 6H-B, and 3C phases, respectively, which are used here as lattice standards. For the 6H-B phase, a Schottky anomaly due to 1.7% of Ni^{2+} orphan spins was also subtracted; see the Supplemental Materials [27]. For the 6H-A phase, C_M shows a sharp peak around $T_N = 13.5$ K. On the other hand, for both the 6H-B and the 3C phases, C_M, which emerges from around 30 K, shows a broad peak around 13 K with no sign for long-range magnetic order down to $T = 0.35$ K. For the 6H-B and the 3C phases, C_M is not at all affected by the application of a magnetic field as large as $H = 9$ T. Below 30 K, the associated change in magnetic entropy (inset in Fig. 3) is 5.0, 3.7, and 2.0 J/mol K for the 6H-A, 6H-B, and the 3C phase, respectively. These values correspond, respectively, to 55%, 41%, and 22% of $R \ln(3)$ for a $S = 1$ system, where R is the gas constant. The remarkable result is that C_M at low temperatures for all three phases follows a γT^α behavior but with a distinct value of α for each phase. As shown in Fig. 3, a linear fit of C_M plotted in a log-log scale yields, respectively, $\gamma = 2.0(1)$ mJ/mol K^4 and $\alpha = 3.0(2)$ for the 6H-A phase in the range $1.8 \leq T \leq 10$ K, $\gamma = 168(3)$ mJ/mol K^2 with $\alpha = 1.0(1)$ for the 6H-B

phase when $0.35 \leq T \leq 7$ K, and $\gamma = 30(2)$ mJ/mol K^3 with $\alpha = 2.0(1)$ for the 3C phase within $0.35 \leq T \leq 5$ K.

Both the susceptibility and the specific heat show no evidence for magnetic ordering down to $T = 0.35$ K for either the 6H-B or the 3C phase, despite moderately strong antiferromagnetic interactions. The 41% (6H-B) and the 22% (3C) changes in magnetic entropy also indicates a high degeneracy of low-energy states at low temperatures. These behaviors suggest that both the 6H-B and 3C phases are candidates for spin-liquid behavior. For the 6H-A phase, the $C_M \propto T^3$ behavior observed below T_N is typical for 3D magnons [29]. This indicates that, besides the intra-layer magnetic interactions within the Ni^{2+} triangular lattice, the interlayer coupling is also relevant for this phase. As for the 6H-B phase, on the other hand, the relative shift of the two nearest Ni^{2+} triangular layers leads to a frustrated interlayer magnetic coupling, which prevents 3D long-range magnetic order. The linear-T-dependent C_M of the 6H-B phase is unusual for a magnetic insulator having a 2D frustrated lattice. Naively, for a 2D lattice, one would expect C_M to display a T^2 dependence given by a linearly dispersive low-energy mode [20].

In fact, a series of recent low-temperature studies reveal that $C_M \propto \gamma T$, with a considerably large value for γ, is a common feature among QSL candidates [12,30,31]. For example, κ-(BEDT-TTF)$_2$Cu$_2$(CN)$_3$ [12], EtMe$_3$Sb[Pd(dmit)$_2$]$_2$ [30], and Ba$_3$CuSb$_2$O$_9$ [31], all composed of a $S = 1/2$ triangular lattice, display $\gamma = 12.0$, 19.9, and 43.4 mJ/mol K^2, respectively. It has been proposed theoretically that magnetic excitations or quasi-particles called spinons can lead to a Fermi surface even in a Mott insulator, which yields a linear term in the specific heat after the U(1) gauge fluctuation is suppressed due to partial pairing on the Fermi surface [32]. The observation of a saturation in $\chi(T)$ for 6H-B phase enables us to calculate the Wilson ratio $R_W = [4\pi^2 k_B^2 \chi_0]/[3(g\mu_B)^2\gamma]$. One obtains a value of 5.6 by using $\chi_0 = 0.013$ emu/mol and $\gamma = 168$ mJ/mol K^2. In metals, a Pauli-like paramagnetic susceptibility and a linear-T-dependent heat capacity, as seen for the 6H-B phase at lower temperatures, which leads to a concomitant R_W in the order of unity, are conventional properties of Fermi liquids. Therefore, we are led to conclude that coherent fermionic like excitations or quasiparticles, which in an insulator can be only magnetic in nature such as the spinons, are responsible for the low-temperature behavior of the 6H-B phase.

It is known that the ground state of quantum $S = 1$ magnets depends on the detailed competition between Heisenberg and biquadratic spin couplings [21,22]. Therefore, although NiGa$_2$S$_4$ and the 6H-B phase both have similar triangular lattice structure and spin 1 on each site, their ground states can be very different. The ground state of NiGa$_2$S$_4$ has quadrupolar order [21,22]
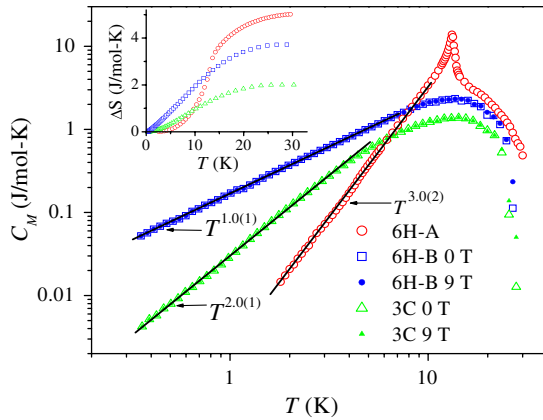
FIG. 3 (color online). (a) Temperature dependencies for the magnetic specific heat (C_M) for all three Ba$_3$NiSb$_2$O$_9$ polytypes. Solid lines are the fits as described in the main text. Inset: Variation in magnetic entropy ΔS below 30 K.

with $C_M \propto T^2$, while in $Ba_3NiSb_2O_9$ we believe it is the spinon Fermi surface that leads to the constant χ and γ at zero temperature.

For the 3C phase, despite diluting nonmagnetic Sb^{5+} ions on the Ni sites, the magnetic interactions between Ni^{2+} ions are still moderately strong indicated by a $\theta_{CW} = -182.5$ K, and it exhibits significant magnetic entropy at low temperatures. If its frustration is due to the site disorder, then one should expect a rather small θ_{CW} for the 3C phase with no magnetic entropy at low temperatures because, normally, the large site disorder from nonmagnetic ions will suffice to interrupt the magnetic interactions suppressing any magnetic phase transition and its concomitant magnetic entropy [33]. The spin-liquid-like ground state then is possibly led by the geometrically frustrated edge-shared tetrahedra composed of $Ni_{2/3}Sb_{1/3}$ sites. The 3C phase crystallizes in a 3D instead of a 2D lattice, and therefore the T^2 dependence observed for C_M is also unconventional. $Na_4Ir_3O_8$, with a 3D $S = 1/2$ (Ir^{4+}) hyperkagome lattice [23], also displays a $C_M \propto T^2$ behavior at low T's, which is claimed to be strong evidence for a QSL ground state and is explained in terms of a spinon Fermi surface [34], which is unstable against a spinon pairing state with line nodes at low energies [35]. A similar scenario could be pertinent for the 3C phase with a face centered cubic structure in which the nearest-neighbor exchange interaction J_1 between the [000] and $[1/2, 1/2, 0]$ spins on the network of edge-sharing tetrahedra is the dominant interaction with a second-neighbor exchange interaction J_2 along the [100] wave vector being the weaker one. Former studies on the double-perovskite $Ba_2MM'O_6$ already showed that the competition between J_1 and J_2 can lead to interesting frustrated magnetic ground states, such as the valence bond glass state in Ba_2YMoO_6 [36].

Gapless QSLs are claimed to exist in 3D lattices or be composed of spins larger than $S = 1/2$. For instance, for spin-S systems, the spin model can be tuned to a $SU(2S + 1)$ invariant point, where quantum fluctuation is significantly enhanced, and the semiclassical spin order is suppressed. Here, we revealed two unique QSL candidates: (i) the $6H$-B phase of $Ba_3NiSb_2O_9$ having a $S = 1$ moment on a triangular lattice and displaying $C_M \propto \gamma T$ with a giant $\gamma = 168$ mJ/mol K^2, therefore suggesting the realization of a ground state with a possible spinon Fermi surface but on a $S = 1$ system, and (ii) the 3C phase of $Ba_3NiSb_2O_9$ with an edge-shared tetrahedral lattice, displaying $C_M \propto \gamma T^2$, thus suggesting a rare example of a 3D QSL composed of $S = 1$ moments. These results show that gapless spin liquids with $S = 1$ exhibit behavior which is akin or has been predicted for $S = 1/2$ systems. This will certainly stimulate further experimental and theoretical work on gapless spin liquids.

*zhou@magnet.fsu.edu
[1] L. Balents, Nature (London) **464**, 199 (2010).
[2] R. Moessner and A. P. Ramirez, Phys. Today **59**, No. 2, 24 (2006).
[3] Ch. Rüegg et al., Phys. Rev. Lett. **95**, 267201 (2005).
[4] Ch. Rüegg et al., Phys. Rev. Lett. **101**, 247202 (2008).
[5] S. H. Lee et al., J. Phys. Soc. Jpn. **79**, 011004 (2010).
[6] G. Y. Xu et al., Phys. Rev. Lett. **84**, 4465 (2000).
[7] M. Kenzelmann et al., Phys. Rev. Lett. **90**, 087202 (2003).
[8] T. Hong et al., Phys. Rev. Lett. **105**, 137207 (2010).
[9] B. D. Gaulin et al., Phys. Rev. Lett. **93**, 267202 (2004).
[10] J. S. Gardner et al., Phys. Rev. Lett. **82**, 1012 (1999).
[11] M. Kenzelmann et al., Phys. Rev. Lett. **87**, 017201 (2001).
[12] S. Yamashita et al., Nature Phys. **4**, 459 (2008).
[13] M. Yamashita et al., Nature Phys. **5**, 44 (2008).
[14] M. Yamashita et al., Science **328**, 1246 (2010).
[15] T. Itou et al., Nature Phys. **6**, 673 (2010)..
[16] J. S. Helton et al., Phys. Rev. Lett. **98**, 107204 (2007).
[17] S. H. Lee et al., Nature Mater. **6**, 853 (2007).
[18] Y. Okamoto et al., J. Phys. Soc. Jpn. **78**, 033701 (2009).
[19] Z. Hiroi et al., J. Phys. Soc. Jpn. **70**, 3377 (2001).
[20] S. Nakatsuji et al., Science **309**, 1697 (2005).
[21] E. M. Stoudenmire, S. Trebst, and L. Balents, Phys. Rev. B **79**, 214436 (2009).
[22] Subhro Bhattacharjee, V. B. Shenoy, and T. Senthil, Phys. Rev. B **74**, 092406 (2006).
[23] Y. Okamoto et al., Phys. Rev. Lett. **99**, 137207 (2007).
[24] Von. U. Treiber et al., Z. Anorg. Allg. Chem. **487**, 161 (1982).
[25] Y. Doi et al., J. Phys. Condens. Matter **16**, 8923 (2004).
[26] P. D. Battle et al., J. Solid State Chem. **85**, 144 (1990).
[27] See Supplemental Material at http://link.aps.org/supplemental/10.1103/PhysRevLett.107.197204 for structural parameters and the specific heat data analysis.
[28] R. L. Carlin, Magnetochemistry (Springer, Berlin, 1986), Chap. 4.
[29] J. A. Gotaas, J. S. Kouvel, and T. O. Brun, Phys. Rev. B **32**, 4519 (1985).
[30] S. Yamashita et al., Nature Commun. **2**, 275 (2011).
[31] H. D. Zhou et al., Phys. Rev. Lett. **106**, 147204 (2011).
[32] S. S. Lee, P. A. Lee, and T. Senthil, Phys. Rev. Lett. **98**, 067006 (2007).
[33] H. D. Zhou et al., Phys. Rev. B **74**, 094426 (2006).
[34] M. J. Lawler et al., Phys. Rev. Lett. **101**, 197202 (2008).
[35] Yi Zhou et al., Phys. Rev. Lett. **101**, 197201 (2008).
[36] M. A. de Vries, A. C. Mclaughlin, and J. W. G. Bos, Phys. Rev. Lett. **104**, 177202 (2010).